Behavior of stimulus response signals in a rat cortical neuronal network under Xe pressure

T. Uchida,* T. Kubota,# R. Tanabe,+ K. Yamazaki, and K. Gohara

Division of Applied Physics, Faculty of Engineering, Hokkaido University, N13 W8 Kita-ku, Sapporo 060-8628, Japan

* Corresponding author. Tel/Fax: +81-11-706-6635, E-mail address: t-uchida@eng.hokudai.ac.jp

Present affiliation: Nittetsu Hitachi Systems Engineering, Inc., tatuya9428@gmail.com

+ Present affiliation: Niigata Prefectural Niigata Minami High School, ru_to6@yahoo.co.jp

Abstract

Neurons cultured on a multi-electrode array show not only spontaneous firing, but also network-specific burst firing, the latter of which develops into synchronous bursting. Such synchronous bursting can be suppressed by exposure to xenon (Xe) gas. To better understand such suppression of bursting by Xe, we investigate here whether signal transmission between neurons is also suppressed under these conditions. In these experiments, we apply a pulse electrical-stimulus to one electrode and observe the response signals within 10 ms at other active electrodes. When put under a sufficient Xe pressure, some response signals become delayed or vanish after disappearance of synchronous-bursts, particularly signals passing through multiple synaptic bonds. Such bonds have a high probability of having delayed or vanishing signals when the Xe pressure is above 0.3 MPa. The pressure dependence of the response ratio to the stimulus suggests that Xe suppresses multiple points of action simultaneously when suppressing synaptic signal transduction, as observed in the suppression of the synchronized bursting. In addition, we find that the signal that transmits not via synaptic bonding (axon conduction) is also suppressed under Xe gas pressures over 0.3 MPa. Therefore, we conclude that Xe-induced suppression of synchronized bursting is caused mainly by a decrease in the apparent number of active neurons that contribute to the neuronal network, a decrease due to inhibition of signal transmission via synaptic connections.
(221 words)

Keywords: maximum of 6 keywords
multi-electrode array, xenon (Xe) pressure, pulse electrical stimulus, synaptic signal transduction, Hill equation

Abbreviations:
Xe, xenon; MEA, multi-electrode array; MD, molecular dynamics; MED, multi-electrode dish; SALPA, Subtraction Artifacts by Local Polynomial Approximation; SBR, synchronized burst rate; NMDA-R, N-methyl-D-aspartate receptor; APV, (2R)-amino-5-phosphonovaleric acid;

Introduction

Several hypotheses have been proposed for the mechanism of general anesthesia by gases. The first one proposed was the “lipid solubility-anesthetic potency correlation", or the Meyer-Overton correlation (Meyer, 1937; Overton, 1901). According to this hypothesis, the anesthetic gas molecule dissolves in the cell membrane, inhibiting the fluidity of the cell membrane and inhibiting the movement of transmembrane ion channels, thereby suppressing the activity of neurons. Later, realizing that most anesthetic gases can form clathrates, Pauling and Miller proposed the "clathrate theory" (Pauling, 1961; Miller, 1961). In their theory, they suggested that the dissolved gas formed clathrates at synapses, thus inhibiting the diffusion of neurotransmitters and signal transmission between neurons. However, due to problems with both hypotheses, two newer hypotheses have become more popular. In the "hydrophobic pocket theory" (Franks and Lieb, 1994), the anesthetic gas binds to the hydrophobic part of an excitatory synapse receptor and acts as an antagonist. More recently, the "K^+ channel activation theory" has been proposed (Franks and Lieb, 1999; Gruss et al., 2004; Pavel et al., 2020), in which the 2-pore-domain K^+ channel is activated, thus suppressing the activity of neurons. However, as neither theory is decisive, the mechanism of general anesthesia continues to be researched.

One difficulty in understanding the mechanism of general anesthesia is our limited understanding of consciousness in the brain. One approach to understanding such brain function focuses on the activity of a single neuron in a neuronal network (Gray and McComick, 1996). Other approaches involve studying the mechanisms of a single neuron firing and the conduction in axon (e.g., Delcomyn, 1997), signal transmission through synaptic connections (e.g., Franks and Lieb, 1999), synchronized firing phenomena (e.g., Abeles, 1991), burst-firing during network formation between neurons (Ito et al., 2010; 2013), and synchronized-bursting phenomena after the maturation of the neuronal network (e.g., Ben-Ari, 2001; Kamioka et al., 1996).

The multi-electrode array (MEA) is a powerful tool for studying the growth of neuronal-network activities. In one study using the MEA, Ito et al. (2010) found a certain size of neuronal network to be necessary for the occurrence of spontaneous synchronous bursts. In their method, Ito et al. (2010; 2013) cultured dispersed neurons on a petri dish having a large number of electrodes, then measured the field potentials at each electrode having an active neuron. With this setup, they could observe how the neuronal network formed from a dispersed state and discern the predominant process of spontaneous synchronous bursts in vitro.

Uchida et al. (2012) constructed a unique experimental system that incorporated the MEA system into a high-pressure vessel, and observed the electrical activity change of the neuronal network under pressurized xenon (Xe) gas. The addition of 0.3 MPa of Xe gas reversibly suppressed the spontaneous synchronous-bursts from the neuronal network activities while maintaining the spontaneous single-firing. This result cannot be explained by the Meyer-Overton correlation because the Xe did not suppress the firing activity of neurons. In addition, they examined the Xe partial-pressure dependence on the neuronal network activity, finding that the spontaneous synchronous-burst frequency decreased with an increase in the Xe pressure (Uchida et al., 2017). Thus, the experiments showed that Xe dissolved in the culture medium

suppresses the synchronized bursting. Related spectroscopic measurements suggested that Xe dissolved in the cell membrane, changing the characteristics of the cell membrane, and that the water around the cells tended to be structured (Uchida et al., 2015). Such a result agrees with findings from MD simulations (Booker and Sum, 2013). Our goal now is to clarify whether or not Xe inhibits the synaptic signal transmission in the neuronal network under conditions of synchronized bursting.

For this study, we measured changes of the evoked firing in a mature neuronal network by inputting the stimuli to one electrode of the MEA under Xe pressure of 0.1 to 0.5 MPa. Based on these measurements, we show that the addition of Xe suppresses the propagation of the spontaneous firing signals and the bursting in the neuronal network. As our aim is to observe signal transmission between neurons via synapses, we targeted the evoked signals with the early response time, that is, less than 10 ms. These signals belong to the early response categorized by Chiappalone et al. (2008).

Experimental Procedure

The MEA64 system (Alpha MED Scientific, Osaka, Japan) is equipped in a high-pressure vessel of about 770 cm^3 of inner volume (Taiatsu Techno, Saitama, Japan). In this system, about 5×10^3 cells mm^{-2} of dissociated cortex neurons prepared from the pieces of Wistar rat fetal cerebral at embryonic day 17 (Nerve-Cell-Culture System: Sumitomo Bakelite, Tokyo, Japan) are plated onto a poly(ethylenimine)-coated MEA probe (multi-electrode dish (MED) probe, Alpha MED Scientific) in which ITO-wired square platinum black electrodes 50-μm across are lined up at intervals of 250 μm in the center of a petri dish of φ25 mm (Kudoh et al., 2007; Hosokawa et al., 2008; Ito et al., 2010; Uchida et al., 2012; 2017). To help prevent the cells from attaching onto the reference electrodes, and to make the cells concentrate around the electrode area, a cloning ring (inner area of 19.6 mm^2) is used during the plating process (Honma et al., 1988). Neurons plated onto the MED probe are cultured with the culture medium in a CO_2 incubator (maintaining 37 °C, 100% humidity and 5% CO_2: MCD-18AIC, Sharp, Tokyo, Japan). The culture medium consisted of DMEM (Invitrogen-Gibco, Carlsbed, CA, USA) supplemented with 5% fetal bovine serum (Invitrogen-Gibco), 5% horse serum (Sigma–Aldrich, St. Louis, MO, USA), 25 lg/mL insulin (Invitrogen-Gibco), 100 U/mL penicillin, and 100 lg/mL streptomycin (Invitrogen-Gibco) (Ito et al., 2010). The field potential of the cultured neurons is observed daily with the MED64 system. The method for the spike detection and the raster-plot analysis were the same as those of Ito et al. (2010). When the neuronal network matures and the number of synchronous bursts reach their maximum, at about 3~4 weeks of culture, we begin the Xe pressurization experiment. For the burst detection, we used the same algorithm with the previous works (Uchida et al., 2012; 2017) which was shown in Mukai et al. (2003). In the high-pressure vessel, the signal from the 4 × 4 electrodes (500 μm × 500 μm) in the center of the MED probe can be measured. As the evoked signal cannot be measured on the electrode that inputs the stimulus, we can measure the signals of only 15 electrodes. For further details of the apparatus, see Uchida et al. (2012, 2017).

After a sample in which 5×10^3 cells mm^{-2} neurons is seeded in an area of about 20 mm^2 and then cultured for about a week, spontaneous firing can be measured by the MED system. After about two weeks, the total number of spontaneous firings increases, and synchronous firings between several electrodes can also be

observed, a signal that indicates the construction of the neuronal network. At this stage, we can measure the synchronized-burst firings. The changes in the number of spontaneous firings and the number of synchronous bursts depends on the culture days similar to that found in previous studies (Ito et al., 2010; Uchida et al., 2012, 2017). We show an example in Fig. S1. The subsequent culture shows a maximum number of synchronous bursts at about 3–4 weeks after seeding. At this stage, the neuronal network activity has matured, showing synchronized bursting in the 4 × 4 electrodes (in the range of 500 μm × 500 μm) such as shown in Fig. S2. The Xe pressurization experiments are then done at this stage.

In an experiment, the MED probe with a matured neuronal network is placed in a high-pressure vessel in a constant temperature box set at 37 °C (FMU-132I, Fukushima Industry, Osaka, Japan). The field-potential measurement begins from the "Control period" at which both the spontaneous firing and evoked signals are measured for 60 minutes. Subsequently, Xe gas (Hokkaido Air Water, Hokkaido, Japan, purity 99.99%) is added at a partial pressure of 0.1 to 0.5 MPa (total pressure of 0.2– 0.6 MPa), and the field potential is measured for 60 minutes. This period is called the pressurized period. After this period, we simply release the pressurized gas to reach atmospheric pressure, and measure the field potential in the Xe-rich atmosphere for 60 minutes. This is the depressurized stage. Finally, the gas is replaced with atmospheric air, and then the field potential is measured for 60 minutes. This stage is called the air-exchanged stage. We run this series of experiments three times in different cultures and average the data to eliminate the individuality of the cultured samples. As a reference experiment with pressure, we run the same stages with the total air pressure at 0.4 MPa (without Xe). The measured firing signals are distinguished from the spike noise and classified into the single firings and the bursts. The definitions of firing signal, burst signal, and synchronous burst signal are the same as in our previous work (Uchida et al., 2012, 2017).

To measure the evoked signals, a square wave stimulus (Fig. 1) is applied to an electrode at 10, 30, and 50 minutes in each experimental stage. The number of stimulations is 18 times at 0.1 Hz, giving a total stimulus time of 3 minutes. We assume, following Chiappalone et al. (2008), that stimuli below 1 Hz have no effect on the network activity and thus our rate of 0.1 Hz does not change the electrical activity of the observed neuronal network.

As the control condition of the response to the stimulus for a sample, we collected all stimulus responses measured at 10, 30, and 50 minutes in the control stage, and averaged them to obtain the control value. In the signal analysis after pressurization, the evoked signal is obtained by averaging the 18 signals in each time series of the experimental stage. For the evoked signal at 10 minutes after pressurization, this average is denoted P10 and similarly for the other times. We then observe the suppressing process of the evoked signals with time in the pressurized stage by comparing the P10, P30 and P50 values. Signal analyses under decompression and air replacement are also run under the same time series and are analogously indicated with symbols D10–D50 and E10–E50.

For the stimulus response signal, we run the following analysis. First, the field potentials are measured on 15 channels other than the input channel for 30 ms (between 10 ms before and 20 ms after the stimulus

input), and the background noise level is identified from the signal before stimulus. Next, we remove the artifact caused by the stimulus input by applying Wagenaar and Potter's (2002) SALPA method (subtraction artifacts by local polynomial approximation). At each electrode, the stimulus response time $\Delta\tau$ is defined as the difference between the signal input time and the time of the maximum amplitude of the evoked signal. Based on the signal measurement in the control stage, an evoked signal occurs within 10 ms with almost the same $\Delta\tau$ (for the given electrode) after the stimulus input, which is consistent with the method of Kiyokawa et al. (2011). Here and elsewhere, by "almost the same $\Delta\tau$", we mean within ± 0.5 ms. Then, we define the evoked signal as the signal that is observed frequently (more than two times over 18 inputs) within 10 ms with almost the same Δτ. To distinguish between an evoked signal and spontaneous firing, we check the field potential records between the stimulus periods on the same electrode. The first response signal observed after the stimulus input is referred to as the "primary response signal", and thereafter, the later response signals are referred to as secondary, tertiary, and higher-order responses observed within 10 ms after the stimulus input.

For the statistical analysis, we analyze data in each stage that differs significantly from data in the control case ($p < 0.05$) using one-way ANOVA with a Dunnett *post-hoc* test (Microsoft Excel 2010 and BellCurve for Excel).

Results

Synchronized bursting and evoked firing in cultured neuronal network

Consider first a case of a matured culture (Fig. 2) that had shown synchronized bursting, and then underwent the Xe pressure experiments. Although 4 × 4 platinum black electrodes are opaque, each likely is covered by several neurons. The large number of cell nuclei (blue) indicate that non-neuronal cells (glial cells) proliferated during the culture, and the cell culture matured. In general, the density of neurons is typically about 10^1 to 10^2 cells mm^{-2} at this stage.

We examine the response signal on a given electrode due to a stimulus from another electrode. For example, with electrode #2 is the stimulus electrode, the action potential profiles on electrode #11 for 18 such runs are overwritten to verify the response signal (Fig. 3a). In every run, the profile shows an apparent spike about 2 ms after the stimulation (time 0). We define this spike as the primary response signal. After this response, several additional spikes sometimes occur within 10 ms after stimulation. For example, a secondary response often occurs at 4–5 ms. In this way, we identify other "higher-order responses" such as the tertiary response. When the profiles are overlapped, as in Fig. 3(b), one sees little variation in the primary response time $\Delta\tau$. On the other hand, the higher-order responses tend to show more scatter as well as having smaller amplitudes.

In this sample, stimulus response signals occur at 11 of the 15 electrodes (Fig. 4). Their primary-response

times $\Delta\tau$ and amplitudes differ between electrodes, with some electrodes having $\Delta\tau$ of about 1 ms, while others being over 2 ms. In this sample, only three electrodes did not exhibit synchronous bursts (those without a red frame; for details, see Fig. S2), yet two of the three nevertheless show a stimulus response. Conversely, a clear stimulus response occurs in 9 of the 12 electrodes that had synchronous bursts. Therefore, this case shows a strong correlation between the synchronous burst and the stimulus response, although they do not necessarily have a one-to-one correspondence.

We ran similar experiments on at least three other cultured samples to examine the reproducibility of this behavior. In general, the response time should be shorter for shorter distances to the input electrode, but we found that $\Delta\tau$ was not always proportional to the distance (see Fig. 4). This variability arises mainly because there are cases in which a neuron on the stimulus input electrode extended its axons across multiple electrodes as shown in Fig. 2. By binning the individual response times within durations of 0.5 ms, the resulting histogram of $\Delta\tau$ in the control period shows a general decay, but with several peaks (Fig. 5). A fit using Gaussians (Origin 2021 Pro) gives a best fit with three peaks ($R^2 = 0.93$) having $\Delta\tau$ values

$\Delta\tau_1 = 1.73 \pm 0.71$ ms,
$\Delta\tau_2 = 4.07 \pm 0.86$ ms, and
$\Delta\tau_3 = 7.10 \pm 1.22$ ms.

For comparison, we can estimate response times from published axonal transmission rates. Bakkum et al. (2013) found axon transmission rates for rat fetal cortical neurons of 0.2–1.5 m s^{-1}, depending on the location in the axon. Applying this speed to the distance between the electrodes in this study, the expected response times would be 0.1–3.2 ms if $\Delta\tau_1$ is assumed to be the direct stimulus response (no synaptic connections) of the neuron on which the cell body or axon was placed on the stimulus input electrode. However, in signal transmission via chemical synapses, a synaptic delay of about 1 ms occurs. In particular, Katz and Miledi (1965) measured the synaptic delay of the neuro-muscular junction, finding a delay of 0.9 ± 0.3 ms. More recently, Boudkkazi et al. (2011) measured the cortical synaptic delay and found that there was a delay of about 1–2 ms. In Fig. 5, the time difference between the first and second response signals is about 2.3 ms, and that between the second and third signals about 3.0 ms, a result that suggests that the response signals for $\Delta\tau_2$ and $\Delta\tau_3$ were via one or two chemical synapses. Therefore, we argue that the data show two types of stimulus response signals. One is the response signal with $\Delta\tau < 2.5$ ms, directly measured the signal transmitted in the axon without going through the chemical synapse. Another is the response signal with $\Delta\tau \geq 2.5$ ms, which may propagate through one or more chemical synaptic bonds. As the purpose of this study is to observe the effect of signal transmission corresponding to the suppression effect of synchronous bursts by Xe pressurization, we classified the response signals into these two types with $\Delta\tau$ ($\Delta\tau_1$ vs $\Delta\tau_2$ and $\Delta\tau_3$) in the control stage.

Synchronized bursting and evoked firing under Xe pressure

Adding Xe gas at pressure to the cultured neuronal network suppressed the synchronized bursting. In

particular, when the pressure of Xe was 0.1 to 0.2 MPa, the number of synchronous bursts decreased to about 40 to 10% of that in the control period, but did not disappear completely during the pressurization time of 60 min. However, when the Xe pressure exceeded 0.3 MPa, the synchronous burst disappeared completely within 5 min. Despite the disappearance of the bursts, spontaneous firing of the neurons at single electrodes did not disappear at any pressure. Then, when the pressurized Xe was released to atmospheric pressure (the depressurized period), the synchronous bursts did not recover immediately, but instead gradually recovered after about 30 min. The number of synchronized bursts was considerably smaller than that in the control period, and tended to increase little by little until the end of the depressurized period. Finally, when the gas in the vessel was replaced with atmospheric air, the synchronous burst recovered to the same level as the control period within about 10 min. Within the variability between the samples, the recovery process of the synchronized burst was roughly independent on the pressure of Xe. In this way, our findings here are consistent with our previous studies (Uchida et al., 2012; 2017). After doing these consistency checks, we then proceeded to examine the changes to the stimulus response signals after Xe pressurization.

For the same sample and input electrode as above, consider the case with 0.3 MPa Xe pressurization. Results (Fig. 6) show that the stimulus response signals at 10 min after pressurization (P10) are similar to those in the control case in Fig. 3(a). As the synchronous burst signal had already disappeared at this time, we conclude that the signal transmission between neurons is not suppressed simultaneously with the synchronous-burst suppression under the Xe pressure. Thereafter, the stimulus response signal is gradually suppressed from 30 min to 50 min. For example, 30 min after Xe pressure (P30), the primary-response signal observed is delayed ($\Delta\tau \sim 2$ ms) and shows more variation. In addition, the secondary-response signal is considerably suppressed and delayed. After 50 min (P50), not only the secondary-response signals, but also the primary ones, are almost completely suppressed.

Consider the recovery trend in the bottom row of Fig. 6. Almost no response signals occur after depressurizing of the Xe gas, even after 50 min (D50), indicating a type of hysteresis. Then after the air replacement (E30), the response signals suddenly resume, including the higher-order responses. By 50 min after the air replacement (E50), the response signal has recovered to almost the same level as the control stage. These temporal changes with hysteresis are similar to the recovery trend of the synchronous bursts (Uchida et al., 2012; 2017).

To investigate the temporal change of the stimulus responses under Xe pressures, we analyze parameters derived from Fig. 6. One parameter is the average values of the response time $\Delta\tau$, another is ρ_j, the response ratio for stage "j". This response ration ρ_j is the ratio of the number of the response signals observed in the stage j to the number of inputs

$$\rho_j = (\text{number of stimulus responses in stage j})/(\text{number of stimulus inputs in stage j}). \quad (1)$$

Then, to examine the general changes in the stimulus response during the pressurization and depressurized

stages, the same experiments are repeated on three culture samples. When the Xe gas is applied with the same pressure on a different sample, the results generally differ due to differences in the network configuration (the state of connections between the neurons). The results also vary with the length of the culture period before the experiment (3–4 weeks). We averaged the results from these samples for a given distance d between the observation electrode and the stimulus-input electrode.

Here we show an example of the response-ratio ρ and response-time $\Delta\tau$ for the average of three experiments at an Xe pressure of 0.3 MPa. For the evoked signal close to the stimulus at $d = 0.15$ mm (red) in Fig. 7B, the response is both quick, at $\Delta\tau < 2$ ms, as well as being nearly constant through all stages. However, ρ for this signal in Fig. 7A decreases in the pressurizing period (P10–P50) to about 1/3 of the control period's value, but remains nonzero. However, for a signal further away, such as $d = 0.474$ mm (sky blue) in Fig. 7B, the response time $\Delta\tau > 2$ ms in the control period tends to increase, with some fluctuation, before the signal disappears ($\Delta\tau \rightarrow \infty$, or does not satisfy the conditions as a response signal). For this signal, ρ also decreases in the pressurizing period, but vanishes after about 30 min (P30). For cases with a similar trend in $\Delta\tau$, the behavior of ρ is similar, vanishing in P30–P50. Therefore, we find the signal transmission between neurons through synapses to be suppressed by Xe pressurization, through both an increase in the response time as well as a decrease in response ratio. These changes are significant for the signal whose initial response time is longer than 2 ms, whereas an initial response signal of less than 2 ms is not suppressed completely even under Xe pressurization, although its response ratio decreases. This difference may correspond to signal transmission with or without synaptic connections, as discussed later. Furthermore, the results show signal transmission between neurons to be suppressed later than the suppression of the synchronous burst.

When Xe is depressurized and returned to atmospheric pressure, period D10 in Fig. 7A, the evoked signal begins to gradually recover, rapidly returning to the control stage level after the air replacement at E10. Figure 7B shows that the response time gradually decreases, finally returning to a value close to that in the control stage. Most of the suppressed signals do not completely recover during the depressurized period, with some response times being larger than their control values 30 to 50 min after depressurization. When Xe is removed from the gas phase by substituting air, the response ratio recovers rapidly, and the response time of the recovered signal is short with little fluctuation. These recovery processes of the suppressed evoked signal after depressurization have similar behavior to those of the synchronous burst recovery. However, we observed an exceptional response in some electrodes: a response signal suddenly started to appear after the air-replacement, although no evoked signal had been observed at that electrode, neither in the control nor in the depressurized stage. This behavior might be caused by some slight modification of the neuronal network from the Xe-pressurization stage, a behavior also observed in the synchronous bursting experiments (Uchida et al., 2012; 2017).

To show the response characteristics for the recovery under Xe pressure of 0.3 MPa, we made a cumulative distribution of the response time for each stimulus stage (Fig. 8). To standardize the distribution, the total number of response signals in each stage is divided by that in the control stage. Thus, the vertical axis in Fig.

8 corresponds to the average response ratio. In the control stage, the curve increases most rapidly for 1–2.5 ms and in 4–5 ms, which correspond to the primary and secondary responses observed in Fig. 5. Then, at 10 min after pressurization (P10), the response signals of $\Delta\tau \geq 2.5$ ms in the control stage become delayed, with some of them completely vanishing (i.e., response time becoming infinite). By this time, the synchronous bursting had already ceased. At 30 min after pressurization (P30), the number of response signals decreases to about 30% of that of the control stage, and the integrated distribution becomes a steady state in which about 2/3 of the response signals occur within 2.5 ms. About 10% of the response signal recovers after depressurization (D10–30), but further recovery does not occur until the air-replacement stage. After the air replacement, the response signals recover to about 75% of the control stage within 10 min (E10), and returns to almost the same distribution as the control stage by about 30 min after the replacement (E30).

To further understand the effect of pressure on the neuronal network activity suppression, we ran an experiment in which air was added instead of Xe at 0.3 MPa. As this experiment omits the "air replacement stage", it finishes 60 min after depressurization. Details are shown in Supplementary Data B. The result shows that the suppression of the activity and the signal transmission of the neural network was not due to physical pressure, but instead due to the effect of Xe.

To examine the Xe pressure dependence of the response signals, we ran the same analyses under Xe pressures of 0.1–0.5 MPa. Details are given in Supplementary Data C. All response signals are averaged over more than three cultured neuronal networks. To compare each pressure condition having different control values, the obtained ρ_i value is normalized by its control value ρ_c. For the cases with Xe pressures at and above 0.3 MPa (Fig. 9A), ρ/ρ_c begins to decrease at P10, when the pressure is applied ($F_{(0.3\ MPa)} = 19.05$, $p < 0.001$, $\rho/\rho_{c(P10)} = 0.72 \pm 0.10$), becoming a steady state at a value below 0.5 at 30 to 50 min ($\rho/\rho_{c(P30)} = 0.28 \pm 0.09$ to $\rho/\rho_{c(P50)} = 0.21 \pm 0.08$). At Xe pressures of 0.3 to 0.4 MPa, the response signal remains nonzero ($F_{(0.4\ MPa)} = 4.89$, $p < 0.001$, $\rho/\rho_{c(P10)} = 0.33 \pm 0.12$), and $\Delta\tau$ increases at P30 ($F_{(0.4\ MPa)} = 2.62$, $p < 0.05$, $\Delta\tau_{(P10)} = 8.14 \pm 0.52$ ms; Fig. 9B). On the contrary, with 0.5 MPa pressure ($F_{(0.5\ MPa)} = 13.60$, $p < 0.001$), the signals vanish from P30 to D30. Under this condition (0.5 MPa), a small number of response signals have $\Delta\tau$ values over 10 ms, which means that we do not classify them as a response signal. Thus, between P30 and D30, ρ is zero (Fig. 9A) and $\Delta\tau$ has no datapoints (Fig. 9B).

On the other hand, for cases with Xe pressure of 0.1 and 0.2 MPa, the value of ρ/ρ_c decreases less than that for the 0.3 MPa case ($F_{(0.1\ MPa)} = 3.14$, $p < 0.005$; $F_{(0.2\ MPa)} = 0.75$, $p = 0.67$; Fig. 9A), which mean no significant differences through all stages. For these low Xe pressures, $\Delta\tau$ is almost constant through all stages ($F_{(0.1\ MPa)} = F_{(0.2\ MPa)} = 0.19$, $p = 0.99$; $F_{(0.3MPa)} = 0.42$, $p = 0.92$;4 $F_{(0.3MPa)} = 2.62$, $p < 0.05$; Fig. 9B), which indicates that the variation (error bar) arises mainly from the difference between samples.

From these results, we conclude that Xe pressurization causes two distinct changes in the signal transmission between neurons via chemical synapses: 1) missing response (decrease in response ratio) and 2) response delay (increase in response time). These changes are more remarkable at higher Xe pressures.

Discussion

Pressure dependence of stationary response ratio under Xe pressure

Within 10 min of applying Xe pressure, the synchronous bursts would be nearly completely suppressed and soon thereafter would either vanish or became steady. However, the stimulus response signals transmitted via chemical synapses did not disappear simultaneously with the synchronous bursts, although their response ratio ρ decreased and their response times $\Delta\tau$ increased. Then, about 30 to 50 min after pressurization, both ρ and $\Delta\tau$ of the evoked signal became steady.

To help analyze how the evoked signal depends on the Xe pressure, we estimate the steady-state response ratio ρ_{PS} by averaging ρ in the periods 30 to 50 min after pressurization (P30 and P50). For the value of Xe of 0 MPa under pressure, we use the data from the 0.3 MPa air-pressurization experiment. ρ_{PS} decreases with an increase of Xe pressure P_{Xe} like a sigmoidal function ($F = 1610$, $p < 0.001$; Fig. 10). This pressure dependence can be fitted by the Hill equation (Eq. (2)), which assumes that the suppression of the response closely resembles the pressure dependence of the suppression of the synchronous burst rate (Uchida et al., 2017), and that both reactions occur by the effect of Xe. That is,

$$1 - \rho_{PS} = P_{xe}^{n} / (k^{n} + P_{xe}^{n}), \qquad (2)$$

where k and n are constants. We used Origin 2021 Pro to calculate the parameter values ($R^2 = 0.951$), obtaining

$k = 0.24 \pm 0.07$ MPa and
$n = 2.2 \pm 0.9$.

Using this k value, the pressure at which the response ratio is halved is 0.24 MPa. This value is more than twice as high as the 0.1 MPa pressure required for 50% suppression of the synchronized burst rate (SBR) (Uchida et al., 2017). Therefore, the suppression effect of evoked signal transmission between neurons is less sensitive to Xe pressure than the inhibitory effect of synchronous burst. The Hill coefficient n = 2.2 obtained in this study is almost the same as the $n = 2.4 \pm 0.4$ found for the inhibitory effect of synchronous bursts (Uchida et al. 2017). In that previous study, we had argued that the SBR inhibition mechanism involved several suppression points for pressurized Xe in the neuronal network. Similarly, we suggest here that suppression points exist for the evoked signal transmission, with these action points located at the chemical synaptic-junction between neurons.

Relationship between Xe-induced inhibition of synchronized bursting and of evoked firing

In a cultured neural network, SBR is suppressed by (2R)-amino-5-phosphonovaleric acid (APV), which is the N-methyl-D-aspartate receptor (NMDA-R)-antagonist (Maeda et al., 1995; Xiang et al., 2007). Given that Xe

also suppresses the synchronous burst, one of the action points for Xe is considered to be NMDA-R. This hypothesis is supported by experimental results for a single neuron (Franks et al., 1998; de Sausa et al., 2000; Ma et al., 2002; Negale et al., 2005). However, we found that the evoked signal differed from SBR in that the signal propagation continued for about an hour under Xe pressure conditions that would completely inhibit SBR. That is, excitatory signals between neurons can be transmitted even though Xe is thought to act on NMDA-R.. As both NMDA-R and non-NMDA-R are present at excitatory synapses, it is likely that Xe specifically inhibits NMDA-R rather than non-specifically inhibiting both receptors. If both excitatory receptors are inhibited, spontaneous firing of neurons should be suppressed (Xiang et al., 2007). But the spontaneous firing has been observed under Xe pressurization. Franks and Lieb (1994) suggested that Xe inhibited the action of NMDA-R when Xe enters the hydrophobic pocket. This supports the idea that Xe acts via a specific inhibition mechanism. Therefore, we suggest that the transmission of the evoked signal under SBR-inhibiting conditions is mediated by non-NMDA-R, and not inhibited by Xe.

Under Xe pressure of more than 0.3 MPa, the transmission of the evoked signal was gradually suppressed, lagging behind the inhibition of the synchronous burst. The pattern of suppression was that the response ratio decreased, which may be caused by an increase in the refractory period, and the response time increased by varying amounts. To explain these findings, and assuming that Xe inhibits the NMDA-R, we consider two mechanisms:

- The evoked signal transmits along a detour route through non-blocked synapses, thus delaying the response signal.
- Considering that the post-synaptic firing requires a sum of signal input from multiple synapses, Xe reduces the number of excitatory signal inputs from synapses via NMDA-R. Thus, the increase in membrane potential is insufficient, and a longer time is needed to reach the firing threshold.

These possibilities are consistent with the multiple points of action of Xe by Hill constant analysis. That is, for Xe pressurization to suppress excitatory signal transmission between neurons, Xe must suppress synapses via multiple NMDA-Rs simultaneously. For synchronous bursts, having sufficient network activity (i.e., of active neurons) is required (Ito et al., 2010). If so, the rapid decay in a synchronized burst would be caused by the preferential inhibition of higher-order responses. However, focusing on the individual neuron-to-neuron communication, especially on the primary response, the sensitivity to Xe pressure is smaller than the inhibition condition of synchronous bursts, and thus a larger amount of Xe is required to observe the suppression state experimentally.

In this experimental system, the activity condition of the fast-spiking neurons was sometimes observed under Xe-induced inhibition of the network activity (Uchida et al., 2012; 2017). We argue that the activity of the inhibitory neurons increased because the excitatory synapse was suppressed by Xe and the excitatory signal was inhibited. In the following air-exchange stage, on the contrary, the excitatory signal was restored and the burst signal began to be measurable. At that moment, the activity of the fast-spiking neuron was suppressed as in the control stage. Therefore, it is considered that the influence of Xe on the neuronal network activity was reversible and selective to the excitatory synaptic transmission.

In addition to the inhibition of NMDA-R, we consider another possible mechanism by which Xe may suppress signal transmission between neurons. As Xe is a clathrate-forming gas, and has relatively large solubility in water, dissolved Xe molecules might structure the surrounding aqueous solution in the synaptic cleft, thus increasing the viscosity (Uchida et al., 2003; Oyama et al., 2003). Raman spectroscopic observation also suggested the structurization of water in the cultured neurons under Xe pressure (Uchida et al., 2015). If the water in the synaptic junction is structured by dissolved Xe, the increase in membrane potential of postsynaptic neurons will be slowed down because the diffusion and migration rates of transmitters and ions in the synaptic cleft will decrease. As observed in the present study, the response ratio decreased gradually after Xe pressurization. As this phenomenon is difficult to describe by the dissolution rate of Xe (Uchida et al., 2012), it would be caused by the structuring of water. This concept is consistent with the "clathrate theory" (Pauling, 1961; Miller, 1961).

In addition, we observed that the suppressed evoked signals did not recover even 50 min after Xe depressurization. If the NMDA-R was inhibited by the existence of Xe in hydrophobic pockets, it should recover upon release of the trapped Xe. The delay of the signal recovery then suggests that the release of Xe from the NMDA-R pockets may be reduced by a retention of Xe that could be caused by a reduction of the Xe diffusion rate through structured water, such as the cage-like water structures around Xe mentioned above.

Recently, activation of the K^+ channel has attracted attention as the point of action of Xe (e.g., Pavel et al., 2020). If Xe is also involved in K^+ channel activation in addition to inhibition of NMDA-R, hyperpolarization in the membrane of the post-synaptic neurons would increase, which could delay the response time. However, since the stimulation interval is 10 seconds in this study, further investigations are needed to show how much the increase in hyperpolarization of the membrane affects the next firing.

Xe pressure effect on non-synaptic signal transmission

After analyzing the $\Delta\tau \geq 2.5$ms signals, which presumably transmit via a chemical synapse, we now turn to the shorter, and more numerous signals (Fig. 5). These faster response signals are presumed to transmit directly, and not through a synaptic junction. The situation may arise, for example, if an axon across the electrode had contact with the stimulus input electrode. This interpretation is also supported by the transmission rate of a signal between electrodes. In this study, the transmission rate of the faster response signal is estimated at approximately 0.35 m/s. This value coincides well with the reported transmission rate on the axons (Bakkum et al., 2013).

For these fast signals, consider the pressure dependences of the signal propagation parameters ρ/ρ_c and $\Delta\tau$ compared to those in the control period. There is almost no increase in $\Delta\tau$ when Xe is applied at a pressure of up to 0.5 MPa ($F_{(0.1\ MPa)} = 0.01$, $p = 1.0$; $F_{(0.2\ MPa)} = 0.15$, $p = 1.0$; $F_{(0.3\ MPa)} = 0.30$, $p = 0.97$; $F_{(0.4\ MPa)} = 0.22$, $p = 0.99$; $F_{(0.5\ MPa)} = 1.39$, $p < 0.5$; Fig. 11B). However, ρ/ρ_c decreases under Xe pressures above 0.3 MPa ($F_{(0.1\ MPa)} = 1.35$, $p < 0.5$; $F_{(0.2\ MPa)} = 3.18$, $p < 0.05$; $F_{(0.3\ MPa)} = 4.74$, $p < 0.001$ $F_{(0.4\ MPa)} = 2.04$, $p < 0.1$; $F_{(0.5\ MPa)} = 4.70$, $p <$

0.001; Fig. 11A). Therefore, if the Xe pressure is less than 0.3 MPa, the signal propagating in the axon may hardly be affected by the Xe pressurization. Moreover, upon examining the distances between the electrodes to which these fast signals were received, we found they were not always adjacent to each other. It is probable that the reason why the response time is short is not only because the electrode is close to the stimulus input electrode, but also because the stimulus response is also transmitted through axons on electrodes far from the input. This result is supported by the immunofluorescence staining image (Fig. 2) that shows the axons on the stimulus input electrode to be widely elongated.

In the case of Xe above 0.3 MPa, the delay of the fast response signal is small, within the range of the error bar, but the response ratio shows a clear decrease. Although this behavior suggests that the response is due solely to pressure, we know of no previous study indicating that signal propagating in the axon is also affected by Xe pressure. Having $\Delta\tau$ unchanged while ρ decreased for the fast response signals under Xe pressure indicates that Xe may be increasing the refractory state while decreasing the propagation speed. Here, we briefly consider several mechanisms by which Xe may interfere with the signal transmission on the axon.

One mechanism that may explain the observed behavior is that Xe dissolves on the cell membrane and suppresses the action of membrane proteins. Xe that dissolves in the cell membrane may change the fluidity of the membrane in proportion to its pressure (Booker and Sum, 2013; Uchida et al., 2015). Therefore, the Xe may suppress the action of ion channels that contribute to signal transmission and inhibit the propagation of action potentials. This concept is compatible with the "the Meyer-Overton correlation". Another possible mechanism is that Xe may activate the 2-pore-domain K^+ channel of neurons. Xe is thought to activate K2p in physiological concentrations, promote hyperpolarization and reduce the frequency of action potentials (Franks & Lieb, 1999; Gruss et al., 2004; Paval et al., 2020). We found here no effect in the pressure range of 0.1 to 0.2 MPa, but a decrease in response ratio above 0.3 MPa (corresponding to 75% in gas composition). This result is consistent with the results of K2p activation observed in an 80% Xe environment (Gruss et al., 2004).

Conclusions

Rat cortical neurons were cultured on MEA probes and then their interneuron signal transduction was measured. In response to pulse stimulation, we discerned three types of responses within 10 ms: a fast response, presumably without chemical synapse binding, a primary response that occurred later presumably via one synapse binding, and higher-order responses via multiple synapse binding. The behavior of these response signals was observed under Xe pressures from 0.1 to 0.5 MPa. At Xe partial pressures above 0.3 MPa, the spontaneous synchronous bursts were suppressed completely within several minutes, whereas the stimulus response via synaptic connections was gradually suppressed over tens of minutes. Then the suppression effect on the response rate was less sensitive to Xe than the synchronous bursts. The suppression involved the response being missing (a decrease in response ratio) and the response being delayed (an increase in response time). These changes in the response signal to the pulse stimulus

generally increased with the Xe pressure. The higher-order response signals were more sensitive to Xe pressurization. At a partial pressure lower than 0.3 MPa, on the other hand, all signal transmissions between neurons was maintained at a considerable ratio, although the synchronous burst rate is lower.

We found that the Xe pressure dependence of the stimulus response rate fit the Hill equation, similar to that of spontaneous synchronous bursts. This analysis suggested that there are multiple points of Xe suppression, a finding similar to that found previously for synchronous burst suppression. The similarities with the synchronous burst suppression process indicate that the point of action of Xe on neural network activity is mainly through NMDA-R. On the other hand, the difference in time-dependent changes during suppression and recovery suggested the possibility of structuring of synaptic pore water due to dissolved Xe. Therefore, this study shows that the MEA measurements can analyze the signal propagations ranged from the network size (millimeter order) to the synaptic size (molecular order) simultaneously.

We also investigated the fast response signal, which was considered to arise from signal transduction on the axons. The fluorescence microscopic images showed extended axons that crossed over multiple electrodes. This fast response signal had not been reported to be affected by Xe pressure. But we found that the response rate decreased at a pressure of Xe higher than 0.3 MPa, although almost no change was found in the response time. This result indicates that Xe dissolves in the cell membrane, then interferes with membrane fluidity and membrane protein function. Therefore, we argue that Xe suppressed mainly the inter-neuronal signal transmission while also affecting the intra-neuron signal transmission when Xe pressure exceeds 0.3 MPa (0.75 in air composition). As the firing phenomenon of the neuron was maintained even under such conditions, we also argue that the Xe gas does not suppress the activity of the neuron itself, but only suppresses the signal transmission.

Acknowledgments

This work was partly supported financially by a Grant-in-Aid for Scientific Research from the Japan Society for the Promotion of Science (grant numbers 17340125, 23350001, 17K18834 and 26105009). We thank Professor Suguru N. Kudoh, Professor Masafumi Nagayama and Dr. Daisuke Ito for their fruitful discussion on this subject. We would also like to thank Dr. J. Nelson, the editor of Redmond Physical Sciences (www.redmondphysicalsciences.com) for the English language review and valuable comments and suggestions that improved the manuscript.

References

Abeles M (1991) Corticonics: neural circuits of the cerebral cortex. Cambridge Univ. Press, Cambridge, p 298

Bakkum DJ, Frey U, Radivojevic M, Russell TL, Müller J, Fiscella M, Takahashi H, Hierlemann A (2013) Tracking axonal action potential propagation on a high-density microelectrode array across hundreds of sites. Nature Comm 4: 2181. (doi: 10.1038/ncomms3181)

Ben-Ari Y (2001) Developing networks play a similar melody. Trends Neurosci 24: 353-360.

Booker RD, Sum AK (2013) Biophysical changes induced by Xenon on phospholipid bilayers. Biochim Biophys Acta 1828: 1347–1356.

Boudkkazi S, Fronzaroli-Molinieres L, Debanne D (2011) Presynaptic action potential waveform determines cortical synaptic latency. J Physiol 589 (5): 1117-1131.

Chiappalone M, Massobrio P, Marinoia S (2008) Network plasticity in cortical assemblies. Eur J Neurosci 28: 221-237.

Delcomyn F (1998) Foundation of Neurobiology. Freeman WH Co., New York, p 648.

de Sousa SLM, Dickinson R, Lieb WR, Franks NP (2000) Contrasting synapticactions of the inhalational general anesthetics isoflurane and xenon. Anesthesiology 92: 1055–1066.

Franks NP, Lieb WR (1994) Molecular and cellular mechanisms of general anesthesia. Nature 367: 607–614.

Franks NP, Lieb WR (1999) Background K^+ channels: an important target for volatile anesthetics? Nature Neurosci 2: 395-396.

Franks NP, Dickinson R, de Sousa SLM, Hall AC, Lieb WR (1998) How does xenon produce anaesthesia? Nature 396: 324.

Gray CM, McComick DA (1996) Chattering cells: superficial pyramidal neurons contributing to the generation of synchronous oscillations in the visual cortex. Science 274 (5284): 109-113. (10.1126/science.274.5284.109)

Gruss M, Bushell TJ, Bright DP, Lieb WR, Mathie A, Franks NP (2004) Two-pore-domain K+ channels are a novel target for the anesthetic gases xenon, nitrous oxide, and cyclopropane. Mol Pharmacol 65: 443–452.

Honma S, Shirakawa T, Katsuno Y, Namihira M, Honma K (1998) Circadian periods of single suprachiasmatic neurons in rats. Neurosci Lett 250: 157–160.

Hosokawa C, Kudoh SN, Kiyohara A, Taguchi T (2008) Resynchronization in neuronal network divided by femtosecond laser processing. Neuroreport 19: 771–775.

Ito D, Tamate H, Nagayama M, Uchida T, Kudoh SN, Gohara K (2010) Minimum neuron density for synchronized bursts in a rat cortical culture on multi-electrode arrays. Neuroscience 171: 50–61.

Ito D, Komatsu T, Gohara K (2013) Measurement of saturation processes in glutamatergic and GABAergic synapse densities during long-term development of cultured rat cortical networks. Brain Res 1534: 22–32.

Kamioka H, Maeda E, Jimbo Y, Robinson HPC, Kawana A (1996) Spontaneous periodic synchronized bursting during formation of mature patterns of connections in cortical cultures. Neurosci Lett 206: 109-112.

Katz BFRS, Miledi R (1965) The measurement of synaptic delay, and the time course of acetylcholine release

at the neuromuscular junction. Proc R Soc Lond B Biol Sci 161: 483-495.

Kiyohara A, Taguchi T, Kudoh SN (2011) Effects of electrical stimulation on autonomous electrical activity in a cultured rat hippocampal neuronal network. IEEJ Trans Electric Electronic Eng 6 (2): 163-167.

Kudoh SN, Hosokawa C, Kiyohara A, Taguchi T, Hayashi I (2007) Biomodeling system – interaction between living neuronal networks and the other world. J Robot Mech 19: 592–600.

Ma D, Wilhelm S, Maze M, Franks NP (2002) Neuroprotective and neuro toxic properties of the 'inert' gas, xenon. Br J Anesth 89: 739–746.

Maeda E, Robinson HPC, Kawana A (1995) The mechanisms of generation and propagation of synchronized bursting in developing networks of cortical neurons. J Neurosci 15: 6834-6845.

Mayer KH (1937) Contributions to the theory of narcosis. Trans Faraday Soc 33:1062–1069.

Miller SL (1961) A theory of gaseous anesthetics. Proc Natl Acad Sci 47:1515–1524.

Mukai Y, Shiina T, Jimbo Y (2003) Continuous monitoring of developmental activity changes in cultured cortical networks. Electr Eng Jpn 145: 28-37.

Negale P, Metz LB, Crowder CM (2005) Xenon acts by inhibition of non-N-methyl-D-aspartate receptor-mediated glutamatergic neurotransmission in caenrhabditis elegans. Anesthesiology 103: 508–513.

Overton E (1901) Studien über die narkose: Zugleich ein beitrag zur allgemeinen harmakologie. Verlag von Gustav Fischer, JENA, pp 195.

Oyama H, Ebinuma T, Shimada W, Takeya S, Nagao J, Uchida T, Narita H (2003) An experimental study of gas-hydrate formation by measuring viscosity and infrared spectra, Can J Phys 81 (1-2): 485-492.

Pauling L (1961) A molecular theory of general anesthesia. Science 134: 15–21.

Pavel MA, Petersen EN, Wang H, Lerner RA, Hansen SB (2020) Studies on the mechanism of general anesthesia. Proc Natl Acad Sci 117 (24): 13757-13766.

Uchida T, Ohmura R, Nagao J, Takeya S, Ebinuma T, Narita H (2003) Viscosity of aqueous CO_2 solutions measured by dynamic light scattering. J Chem Eng Data 48 (5): 1225-1229.

Uchida T, Suzuki S, Hirano Y, Ito D, Nagayama M, Gohara K (2012) Xenon-induced inhibition of synchronized bursts in a rat cortical neuronalnetwork. Neuroscience 214: 149–158.

Uchida T, Nagayama M, Yamazaki K, Gohara K, Sum AK (2015) Raman spectra measurements on DEPC liposome and cell membrane of living neuron under xenon pressure. Can J Chem 93: 831–838.

Uchida T, Shimada K, Tanabe R, Kubota T, Ito D, Yamazaki K, Gohara K (2017) Xenon pressure dependence on the synchronized burst inhibition of rat cortical neuronal network cultured on multi-electrode arrays. IBRO Reports 3: 45-54.

Wagenaar DA, Potter SM (2002) Real-time multi-channel stimulus artifact suppression by local curve fitting. J Neurosci Meth 120: 113-120.

Xiang G, Pan L, Huang L, Yu Z, Song X, Cheng J, Xing W, Zhou Y (2007) Microelectrode array-based system for neuropharmacological applications with cortical neurons cultured in vitro. Biosensors and Bioelectronics 22: 2478-2484.

Figure captions

Fig. 1. The stimulus input waveform.

Fig. 2. Fluorescence-stained image of the neuronal network cultured on a MED probe used for the Xe 0.3 MPa pressurization experiment. Blue identifies cell nuclei, green regions are dendrites, and red are axons. The scale bar in white and the size of a platinum black electrode (black square with number) is 50 μm.

Fig. 3. Action potential profiles at electrode #11 in Fig. 2, starting 10 ms before each stimulus input. The input is at electrode #2, which is 335 μm away. (A) Each of the 18 action potential profiles. (B) Superimposed profiles. Black is the raw data, and blue is data after SALPA artifact removal.

Fig. 4. Stimulus response signals in each electrode of the 4 × 4 array, except the source electrode (#2) for the same control case of Fig. 3. As in Fig. 3B, black is the raw data, blue is after SALPA processing. The arrow on each electrode marks the primary-response signal. Electrodes that had exhibited synchronous bursts are outlined with a red frame (cf. Fig. S2).

Fig. 5. Histogram of the response time $\Delta\tau$ obtained in the control period. Number of times n = 395. Three peaks are fitted by gaussian (shown by solid, dotted and dashed lines).

Fig. 6. Typical evoked signals on electrode #11 for case of 0.3 MPa Xe pressurization at several stages: P10, P30, P50, D50, E30, and E50. A scheme of the experimental protocol is illustrated with showing the stimulus points.

Fig. 7. Response parameters from evoked signals for case of 0.3 MPa Xe pressurization. A) Average response ratio ρ. Abscissa coordinate gives the stage, with P10–P50 the Xe pressurized stage, D10–D50 the depressurized stage, and E10–50 the air-exchange stage. A scheme of the experimental protocol is illustrated with showing the stimulus points. Depth coordinate is the distance from the evoked electrode. B) Average response time $\Delta\tau$ of evoked signals. The legend is common for both figures showing the distance from the evoked electrode in mm unit.

Fig. 8. Integrated distribution of response time in each stage for the Xe = 0.3 MPa case. The number of responded electrodes is normalized by that at control stage. A scheme of the experimental protocol is illustrated with showing the stimulus points.

Fig. 9. Response to stimulus signal over a range of Xe pressures for the longer signals (i.e., $\Delta\tau \geq 2.5$ ms). A) Average response ratio relative to the control period ρ/ρ_c. B) Response time $\Delta\tau$ of evoked signals. Stages are the same as before: P10–P50: pressurized stage, D10–D50: depressurized stage, and E10–E50: air-exchanged stage. A scheme of the experimental protocol is illustrated with showing the stimulus points. The error bar shows the standard error of all values obtained from all active channels included in different samples under that stimulus condition. Asterisk near a given datapoint marks the case as having a statistically significant difference compared to the value from the control case (* for $p < 0.01$, (*) for $p < 0.05$ by the Dunnett test, in which the significance is determined using one-way ANOVA).

Fig. 10. Steady-state response ratio under various Xe pressures (ρ_{PS}; solid circles). For comparison, the pressure dependence of the spontaneous burst rate (s-SBR; open squares) is also shown. The significant difference of ρ_{PS} from that with no Xe pressure is determined using one-way ANOVA. Both dotted lines show the Hill fitting curve, eq. (2).

Fig. 11. Same as Fig. 9 except for the shorter signals ($\Delta\tau < 2.5$ ms). A scheme of the experimental protocol is illustrated with showing the stimulus points.

Fig. 1.: The stimulus input waveform.

Fig1_82mm

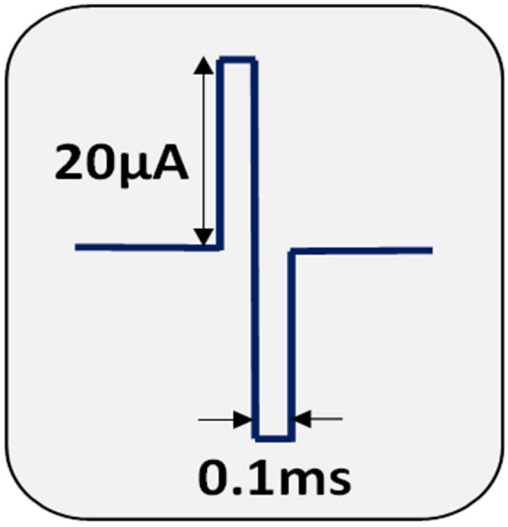

Fig. 2. Fluorescence-stained image of the neuronal network cultured on a MED probe used for the Xe 0.3 MPa pressurization experiment. Blue identifies cell nuclei, green regions are dendrites, and red are axons. The scale bar in white and the size of a platinum black electrode (black square with number) is 50 μm.

Fig2_120mm

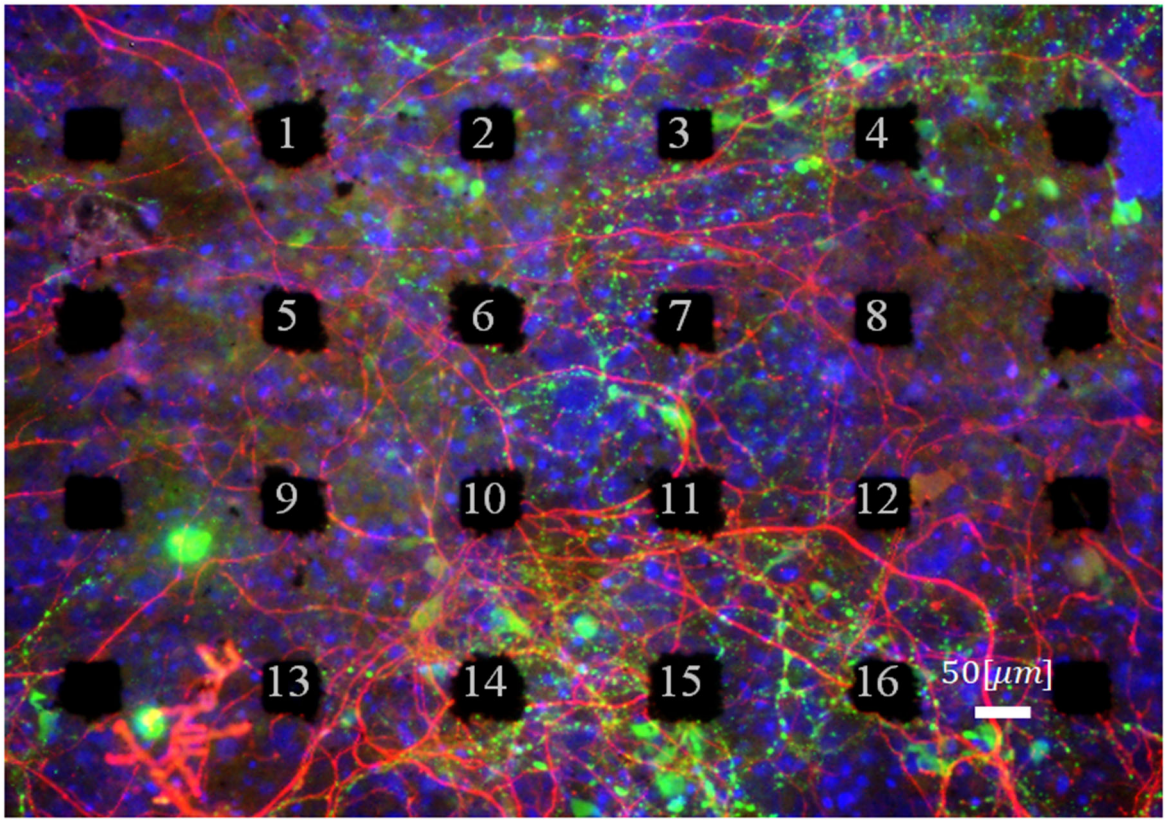

Fig. 3. Action potential profiles at electrode #11 in Fig. 2, starting 10 ms before each stimulus input. The input is at electrode #2, which is 335 μm away. (A) Each of the 18 action potential profiles. (B) Superimposed profiles. Black is the raw data, and blue is data after SALPA artifact removal.

Fig3A_82mm

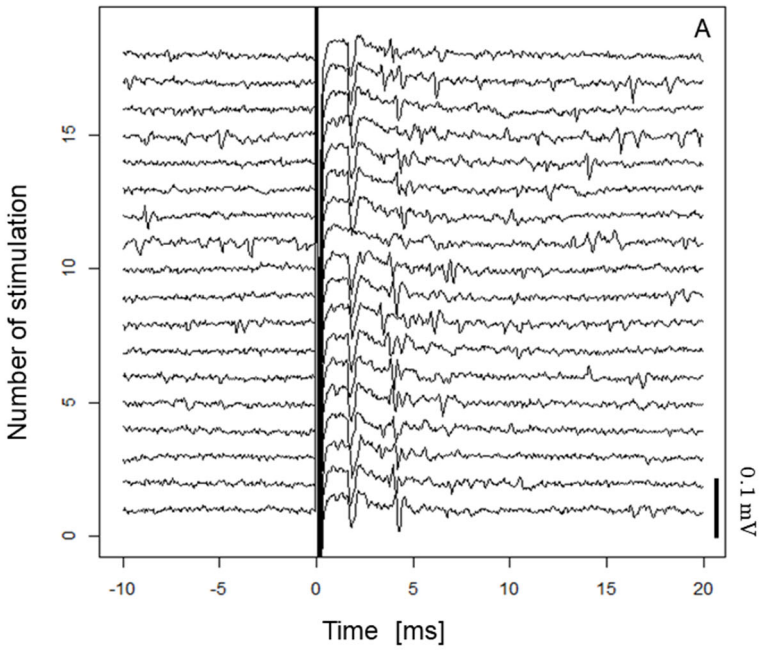

Fig3B_82mm

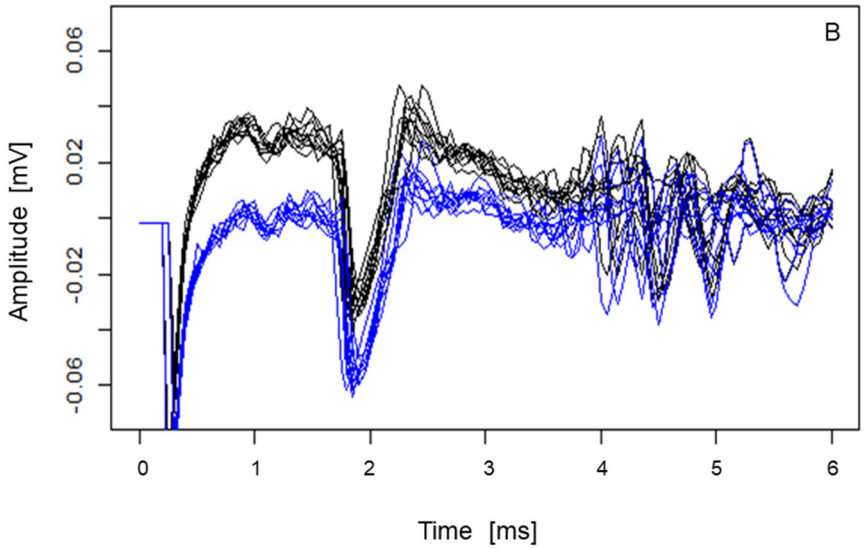

Fig. 4. Stimulus response signals in each electrode of the 4 × 4 array, except the source electrode (#2) for the same control case of Fig. 3. As in Fig. 3B, black is the raw data, blue is after SALPA processing. The arrow on each electrode marks the primary-response signal. Electrodes that had exhibited synchronous bursts are outlined with a red frame (cf. Fig. S2).

Fig4_120mm

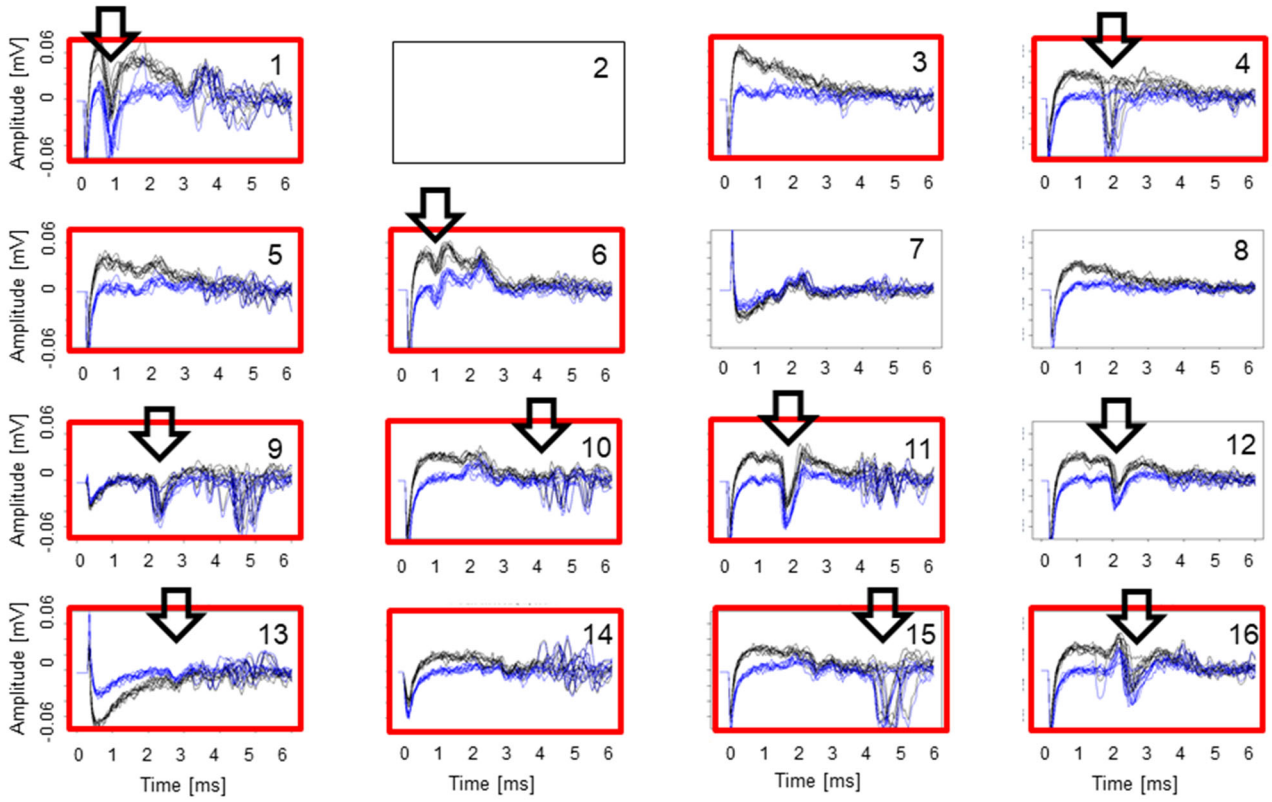

Fig. 5. Histogram of the response time Δτ obtained in the control period. Number of times n = 395. Three peaks are fitted by gaussian (shown by solid, dotted and dashed lines).

Fig5_82mm

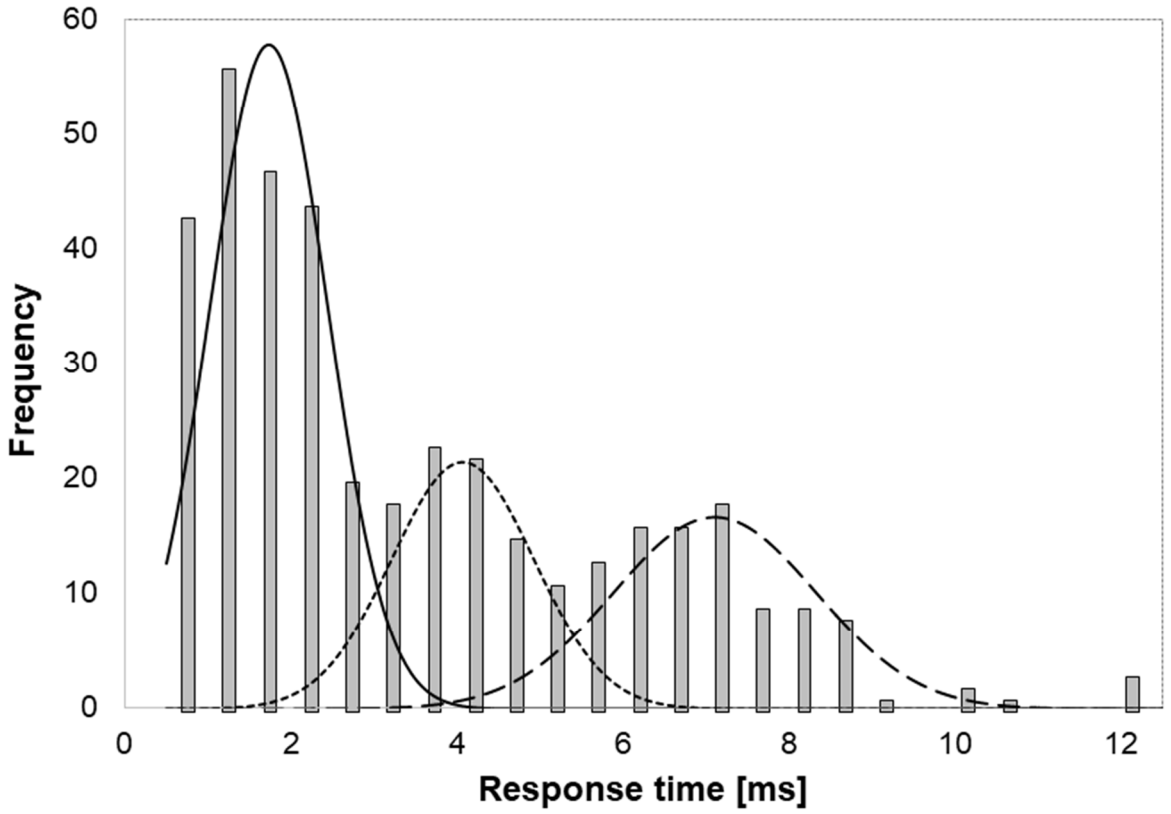

Fig. 6. Typical evoked signals on electrode #11 for case of 0.3 MPa Xe pressurization at several stages: P10, P30, P50, D50, E30, and E50. A scheme of the experimental protocol is illustrated with showing the stimulus points.

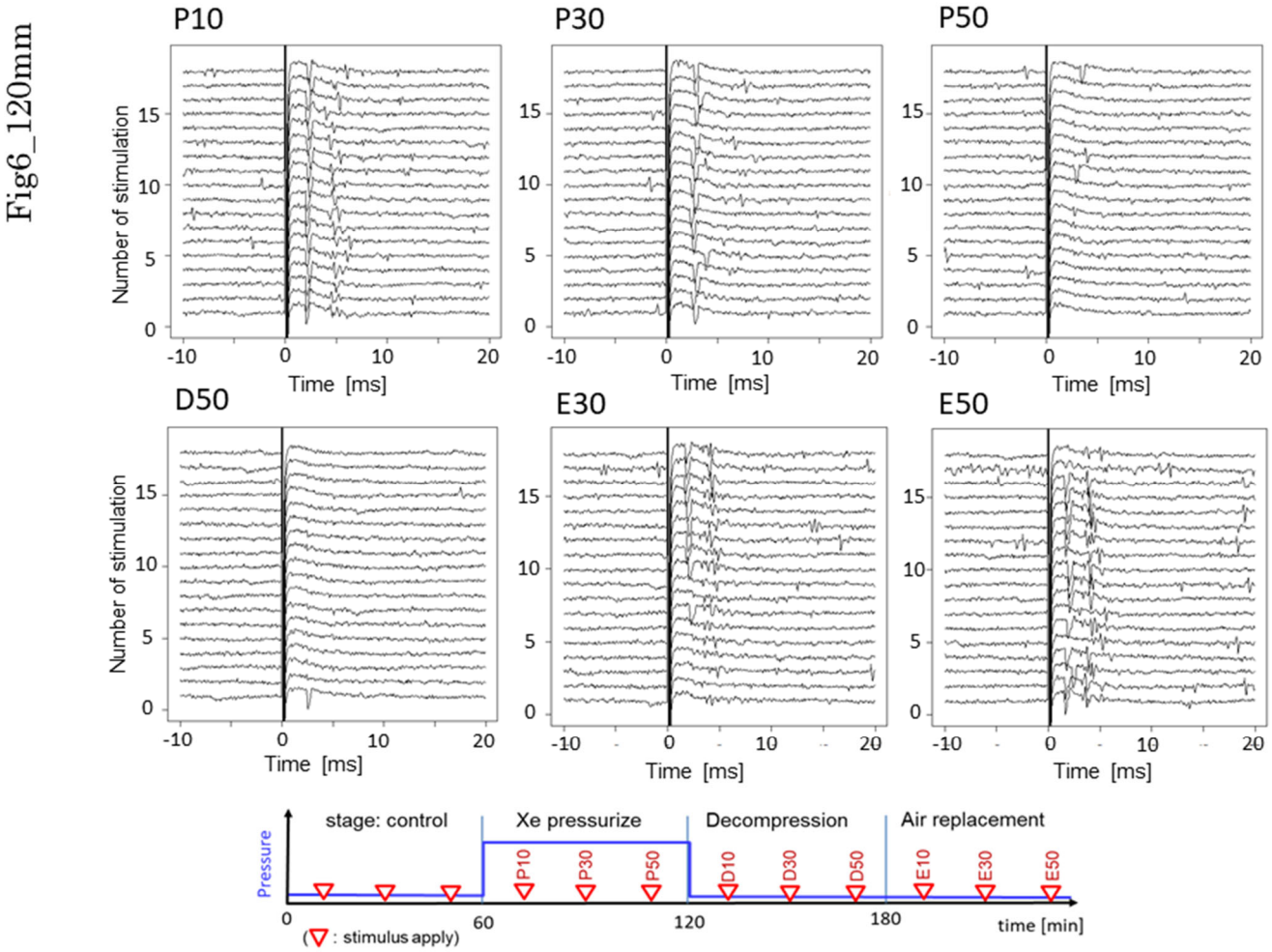

Fig. 7. Response parameters from evoked signals for case of 0.3 MPa Xe pressurization. A) Average response ratio ρ. Abscissa coordinate gives the stage, with P10–P50 the Xe pressurized stage, D10–D50 the depressurized stage, and E10–50 the air-exchange stage. A scheme of the experimental protocol is illustrated with showing the stimulus points. Depth coordinate is the distance from the evoked electrode. B) Average response time $\Delta\tau$ of evoked signals. The legend is common for both figures showing the distance from the evoked electrode in mm unit.

Fig7_120mm

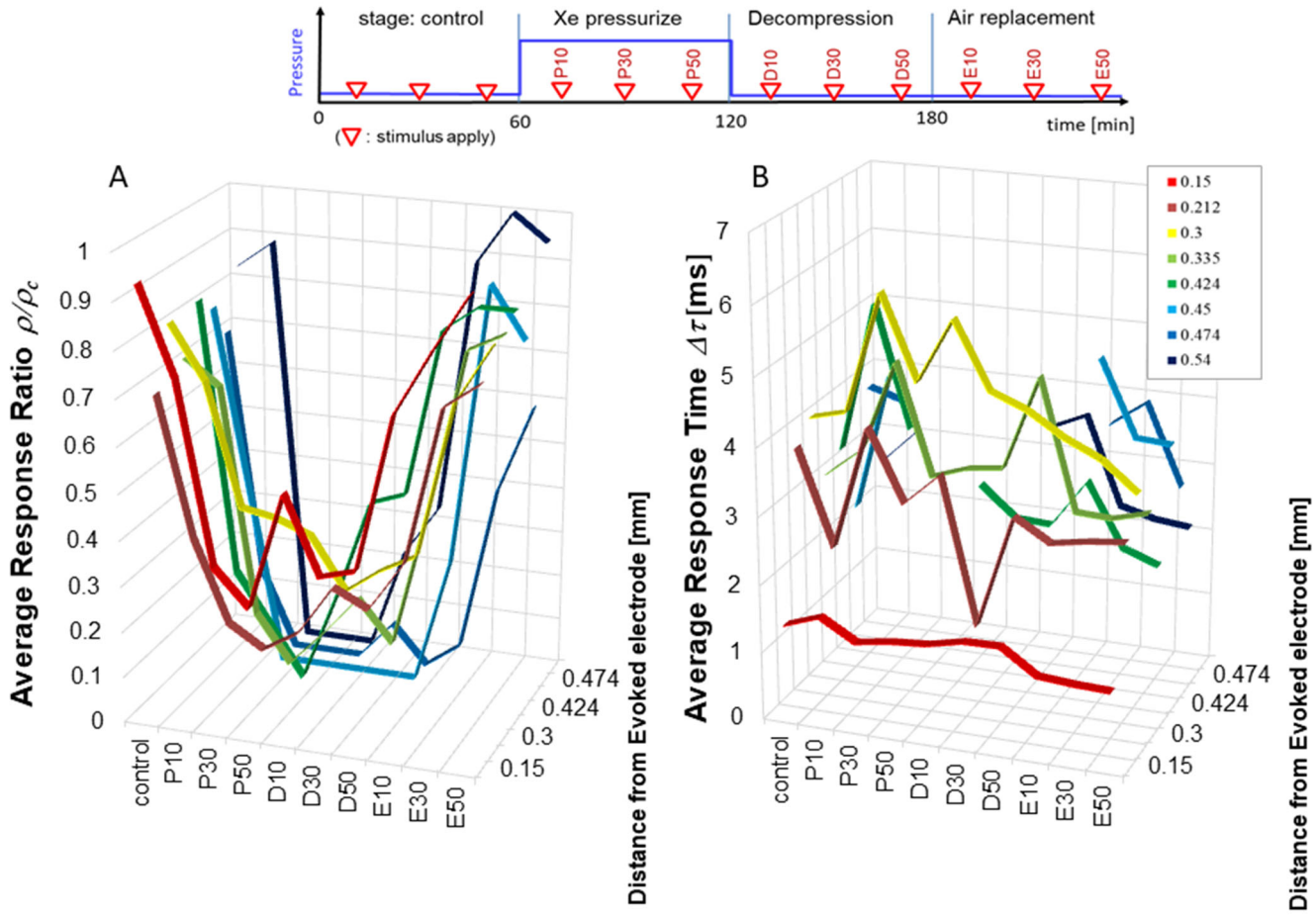

Fig. 8. Integrated distribution of response time in each stage for the Xe = 0.3 MPa case. The number of responded electrodes is normalized by that at control stage. A scheme of the experimental protocol is illustrated with showing the stimulus points.

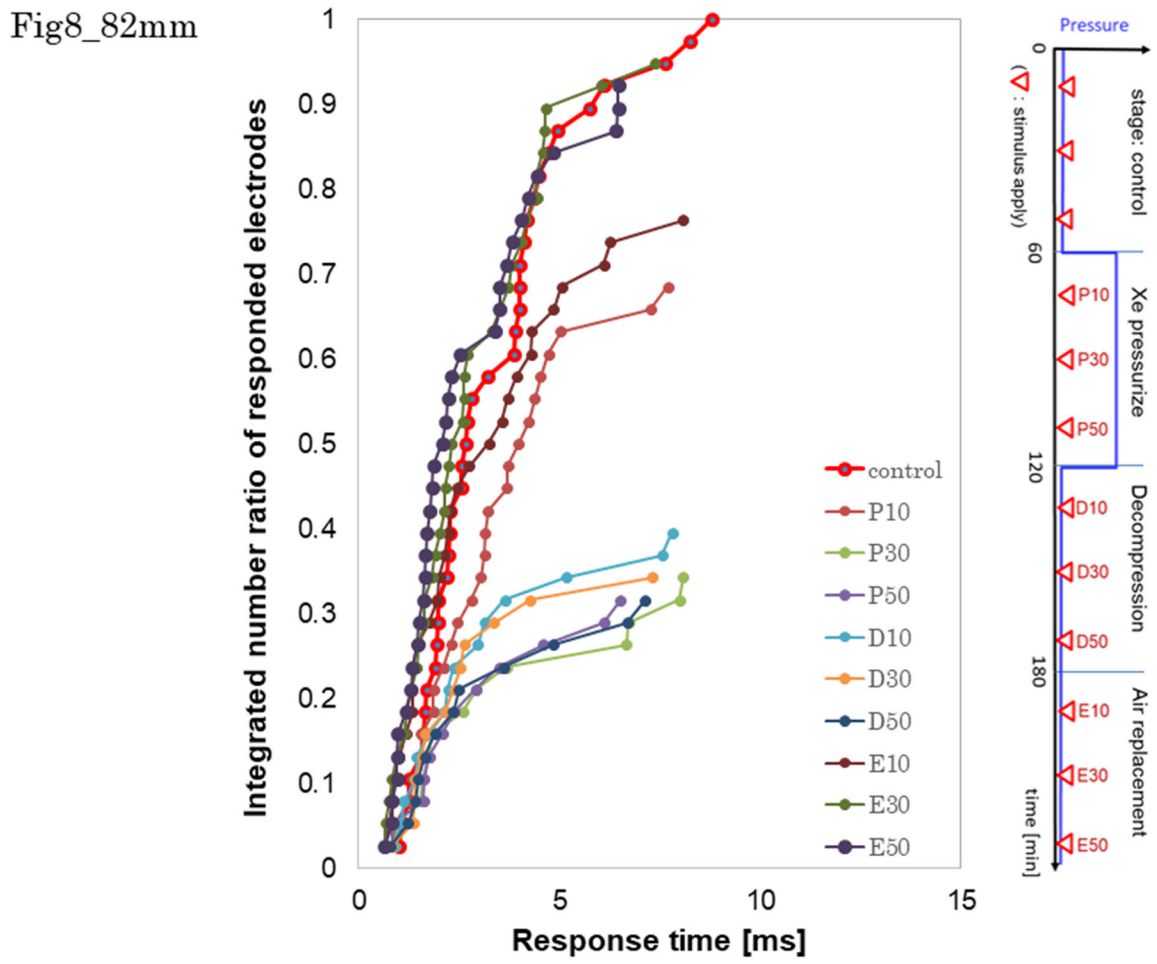

Fig. 9. Response to stimulus signal over a range of Xe pressures for the longer signals (i.e., $\Delta\tau \geq 2.5$ ms). A) Average response ratio relative to the control period ρ/ρ_c. B) Response time $\Delta\tau$ of evoked signals. Stages are the same as before: P10–P50: pressurized stage, D10–D50: depressurized stage, and E10–E50: air-exchanged stage. A scheme of the experimental protocol is illustrated with showing the stimulus points. The error bar shows the standard error of all values obtained from all active channels included in different samples under that stimulus condition. Asterisk near a given datapoint marks the case as having a statistically significant difference compared to the value from the control case (* for $p < 0.01$, (*) for $p < 0.05$ by the Dunnett test, in which the significance is determined using one-way ANOVA).

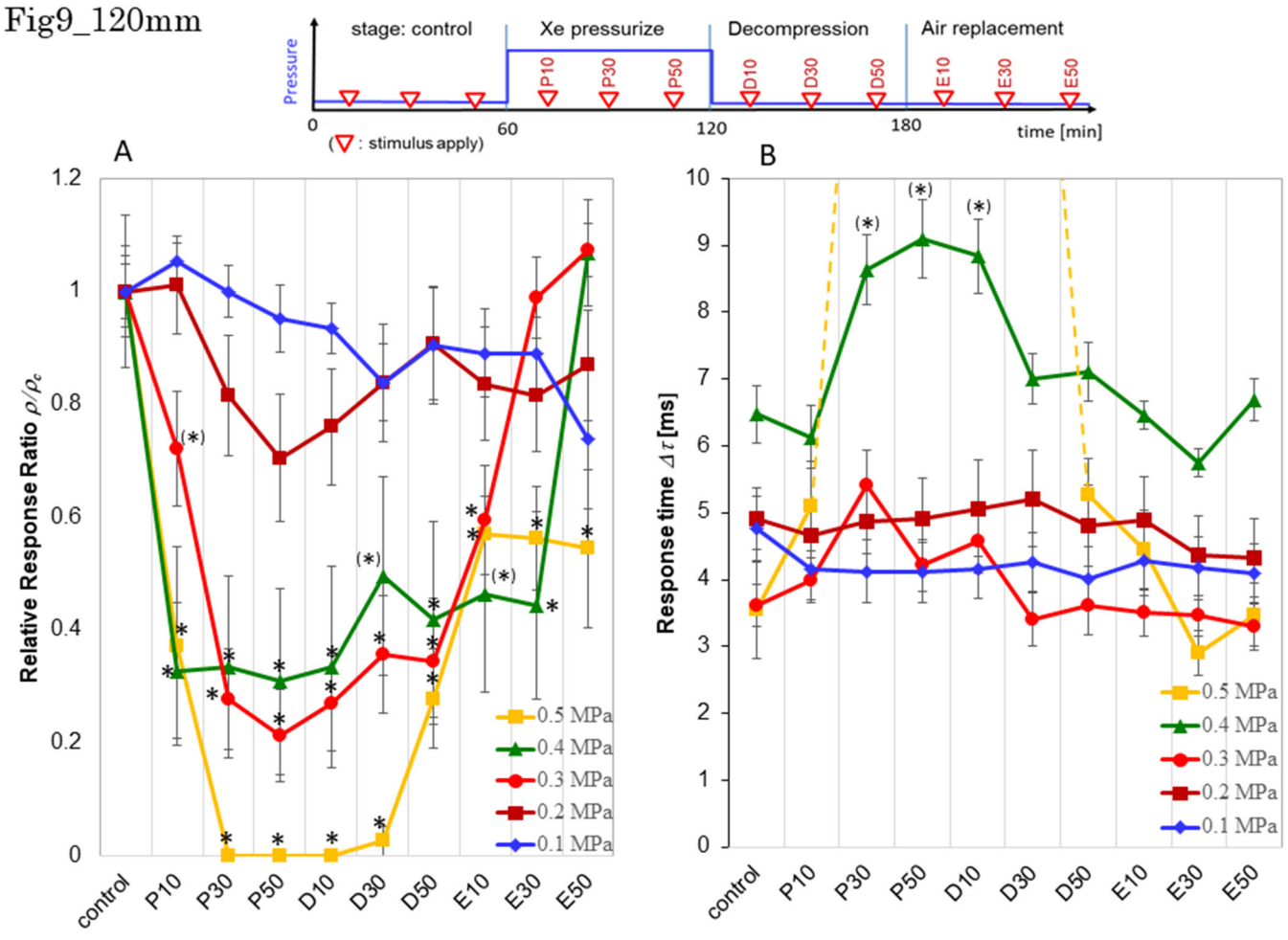

Fig. 10. Steady-state response ratio under various Xe pressures (ρ_{PS}; solid circles). For comparison, the pressure dependence of the spontaneous burst rate (s-SBR; open squares) is also shown. The significant difference of ρ_{PS} from that with no Xe pressure is determined using one-way ANOVA. Both dotted lines show the Hill fitting curve, eq. (2).

Fig10_82mm

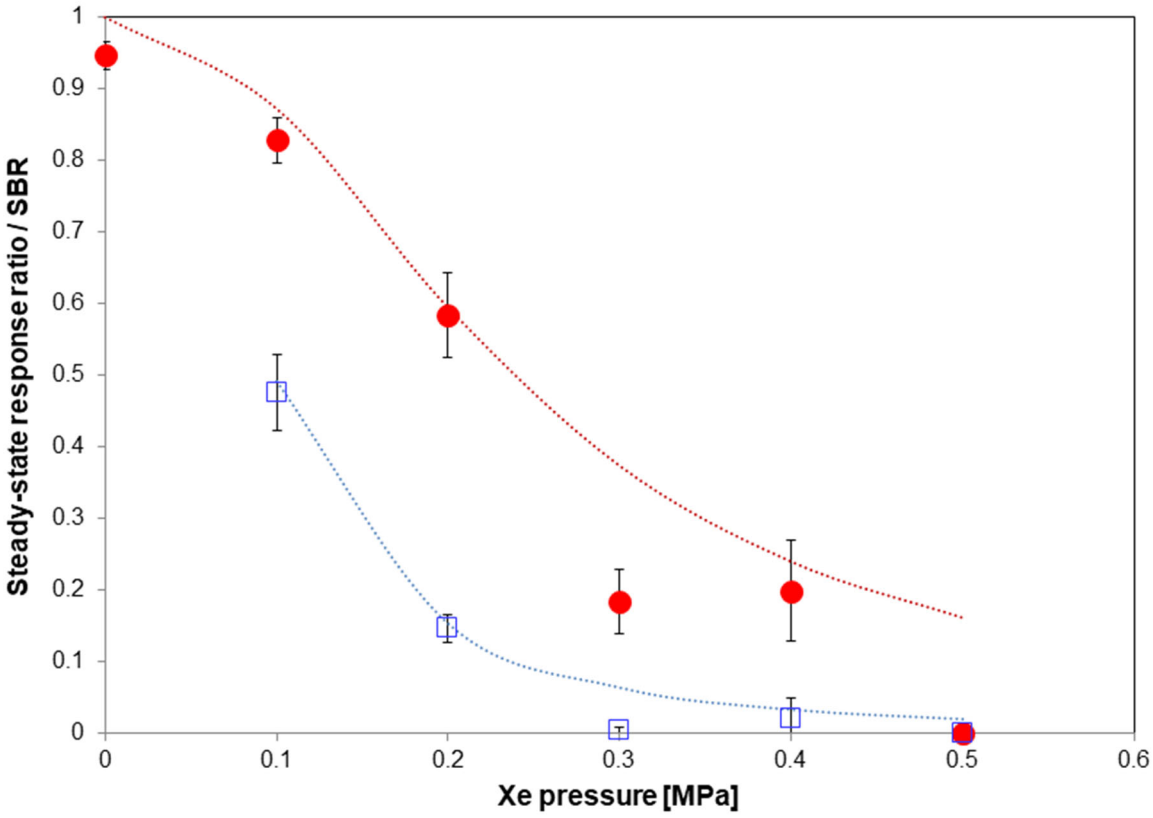

Fig. 11. Same as Fig. 9 except for the shorter signals ($\Delta\tau < 2.5$ ms). A scheme of the experimental protocol is illustrated with showing the stimulus points.

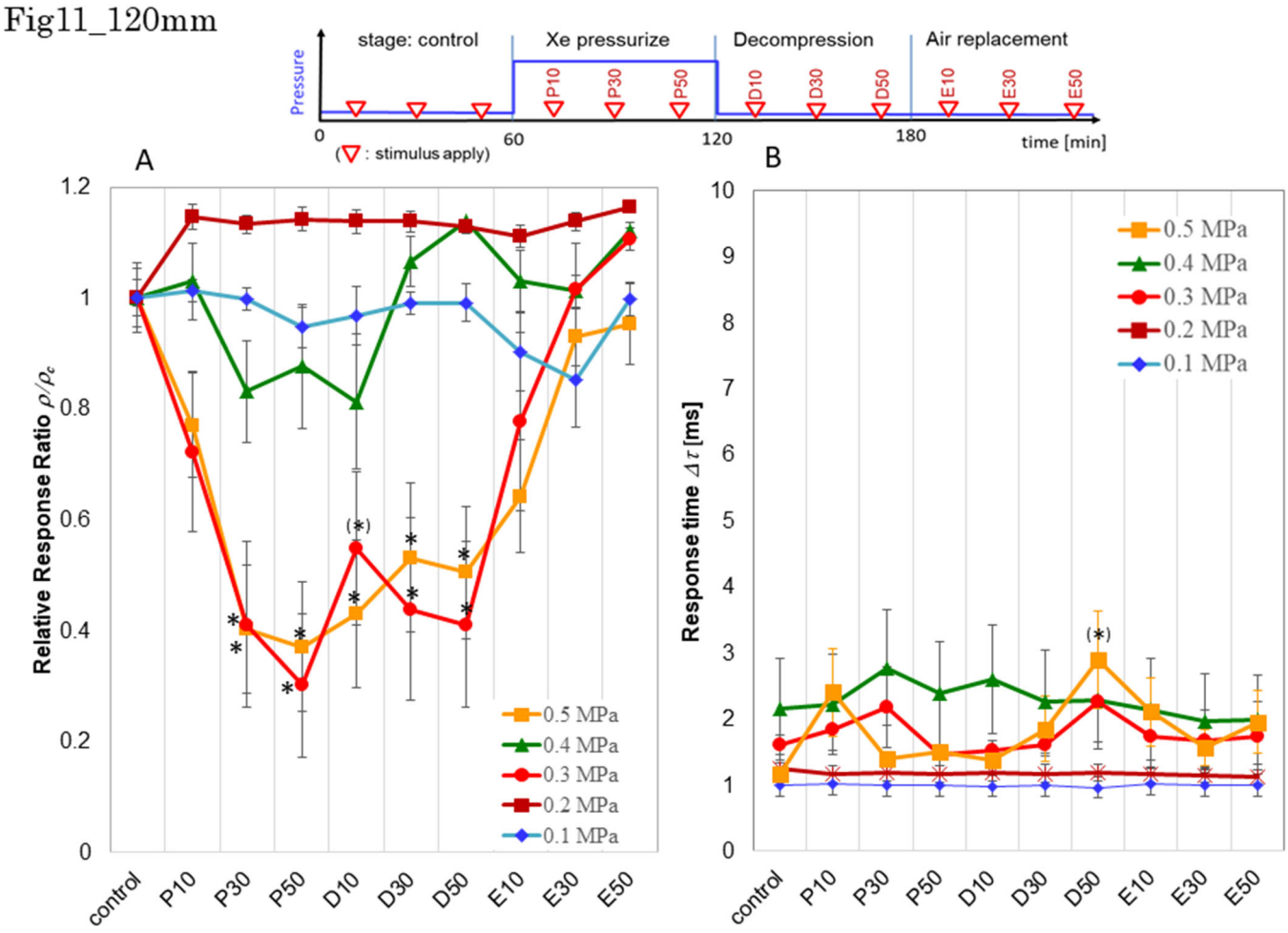

Highlights

1. The stimulus response via synaptic connections is suppressed at Xe pressures above 0.3 MPa. (91 characters)

2. Xe induced suppression of the response rate is less sensitive than that of the synchronous burst. (97 characters)

3. Hill-equation fitting to the Xe pressure dependence of the stimulus response rate shows multiple suppression points. (115 characters)

4. The signal transduction on the axons is also depressed, only in response rate at Xe pressures above 0.3 MPa. (108 characters)

Graphical Abstract (5 × 13 cm)